The Journal of Engine Research

Engine Injector Multiphase Flow with Indicated Quantities Simulation for Different Orifice Geometries and Needle Movements

R. Firuzi [1*], F. Bagherpoor [2], A. Farajollahi [3]

[1] Faculty of Mechanical Engineering, Imam Khomeini International University, Iran, *rezafiruzi@edu.ikiu.ac.ir*
[2] Faculty of Mechanical Engineering, Imam Ali University, Iran, *farid.bagherpor@gmail.com*
[3] Faculty of Aerospace Engineering, Imam Ali University, Iran, *a.farajollahi@sharif.edu*
Corresponding Author

ARTICLE INFO

ABSTRACT

In the present paper, the effect of using Different Orifice Geometries & Needle Lifts on transient heat-mass transfer and Combustion Indicated Quantities & Air Pollutant Species has been investigated in Marine Propulsion System Fuel Injectors using AVL-Fire CFD code. The effect of each of the proposed geometry and needle movement profiles (triangular, trapezius & boot) with the help of a three-dimensional moving mesh by numerical model in AVL Fire software, which has been validated with experimental data in each part, on the performance & Air Pollutant Species of the Marine Propulsion System has been investigated by ANALYSER module. Numerical results show that converged conical with trapezius needle lift profile has better engine performance, efficiencies and low NO pollution. Although, diverged conical with trapezius needle lift profile has lower CO pollution. Fuel consumption decreases by 18.5% and its power and torque increase 64%. Also in this case, carbon monoxide pollutants decrease by 14% and nitrogen oxide pollutants decreasing by 10% for optimum status. In these case, indicated and mechanical efficiencies are increasing 22% and 41.5%, respectively.

1) Introduction

Diesel engines are widely used in the marine industry due to their higher compression ratio, power and torque output, as well as lower fuel consumption than other internal combustion engines. Applications of this type of engine include commercial ships, tourism and various types of surface and submarine vessels. Today, more than 80% of world trade is done by sea. This has made the share of fuel consumption in this sector very significant and more than 3% of the world's carbon dioxide is produced by ships. Marine propulsion systems & diesel engines are shown in Figure 1. Given the increasing use of marine diesel engines and the problems caused by the limited resources of fossil fuels and their pollution, efforts to reduce pollutants and optimize fuel consumption is important and necessary. A variety of fuel delivery systems and proper and timely fuel injection in a diesel engine are the most important factor in improving its efficiency. For this reason, most diesel engine manufacturers have done a lot of research and work in the field of fuel system and have their own methods. Older engines used simple fuel injection technology that replaced the carburetor to overcome some of its shortcomings. The carburetor was a mechanical device that could not completely control a precise fuel-to-air ratio. Hence, they replaced it with a new common rail fuel injection technology in which fuel is atomized (powdered) by injecting it. In this method, with a common rail fueling system, the combustion process can be optimized by producing less pollutants and lower fuel consumption. In diesel injectors, cavitation occurs due to a sudden change in the geometry of the nozzle inlet hole, which leads to a drop in pressure to the vapor pressure of the liquid fuel. In this case, the boundary layer tends to separate and the return flow is created by a high pressure drop. Nozzle inlet geometry, injection pressure, needle lift profile, fuel type as well as its temperature has a great impact on the specifications of the sprayed fuel and the performance of the diesel engine. Fuel injection pressure, starting time, injection rate, nozzles geometries and in-cylinder environment conditions have a great impact on the combustion and emissions of diesel engine [1]. Today, in addition to using different types of fuels and systems to control and regulate pollutant gases in engines, injector nozzle geometry is an important factor in improving fuel quality and engine efficiency [2-4].
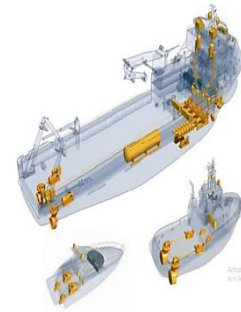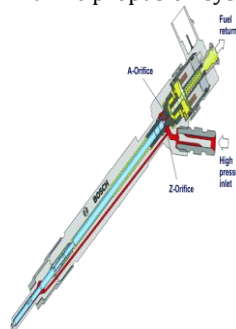

Marine propusion systems   Diesel engine in boats

Fuel injector parts   Marine diesel engine

Figure 1: Marine propulsion systems & diesel engines

In-nozzle flow can be controlled by dynamics, hydrodynamics, and geometric factors that have been extensively studied in terms of injection pressure, two-phase liquid fuel flow in the nozzle, needle lift profile, and orifice geometry [5, 6]. The hydrodynamic behavior of the liquid fuel flow between the inlet nozzle, including cavitation and turbulence, can improve the atomization of diesel fuel injectors [7, 8] and increase the conical angle of the injectors [9, 10]. Given the pollution caused by this type of engine and the limited fossil fuel resources, it is important to try to reduce the pollution caused by this type of engine, reduce fuel consumption and increase combustion efficiency. In fuel supply systems, changing the injector nozzle geometry, needle displacement profile and creating a rotational flow to improve the quality of fuel atomization and better mixing with air, because better mixing of fuel and air will cause better combustion. Occurrence of cavitation phenomenon in high pressure injection systems can be useful for fuel jet development because it can improve the initial decay and fuel atomization. Our high pressure difference between the beginning and the end of the injector orifice, in addition to the geometric

characteristics of the injector nozzle, which increases the flow velocity at the nozzle output, leads to higher dynamic pressure and lower static pressure in the nozzle internal flow and ultimately cavitation growth. It should be noted that the bursting of steam bubbles inside the injector nozzle leads to erosion of the nozzle surface and thus reduces its service life. Therefore, an optimal rate for cavitation is desirable. Changes in fuel supply systems lead to changes in the characteristics of the fuel fountain. Fuel jet characteristics play an important role in the performance of diesel engines and their emissions. Penetration length, average diameter of the cover and cone angle are the most important characteristics of the fuel fountain.

Strotos et al. have been numerically investigated the importance of fuel pressurization, phase-change due to cavitation, wall heat transfer and needle valve motion on the fluid heating induced in high pressure Diesel fuel injectors. Variable fuel properties, being a function of the local pressure and temperature are found necessary in order to simulate accurately the effects of depressurization and heating induced by friction forces. Comparison of CFD predictions against a 0-D thermodynamic model, indicates that although the mean exit temperature increase relative to the initial fuel temperature is proportional to (1-Cd2) at fixed needle positions, it can significantly deviate from this value when the motion of the needle valve, controlling the opening and closing of the injection process, is taken into consideration. Increasing the inlet pressure from 2000 bar, which is the pressure utilized in today's fuel systems to 3000 bar, results to significantly increased fluid temperatures above the boiling point of the Diesel fuel components and therefore regions of potential heterogeneous fuel boiling are identified [11].

Farajollahi et al. have been investigated the effects of creating rotationary flow inside the nozzle and changing fuel injection angle on the performance and emission of caterpillar diesel engine. The numerical results indicate that creating rotationary flow inside the nozzle decreasing penetration length while increasing fuel spray cone angle and improves atomization quality. The nozzle with grooves has better performance and lower emission compared to other geometries. In this case, the fuel consumption is decreasing 37 percent than that of the cylindrical one, while the engine power and its torque increases 75 percent than cylindrical nozzle hole. In addition, the amount of nitrogen oxide (NO) and carbon monoxide for the grooved nozzle geometry reduces 45 and 42 percent respectively than cylindrical nozzle hole [12].

Kolovos et al. have been done an investigation of the fuel heating, vapor formation, and cavitation erosion location patterns inside a five-hole common rail diesel fuel injector, occurring during the early opening period of the needle valve (from 2 μm to 80 μm), discharging at pressures of up to 450 MPa, is presented. Numerical simulations were performed using the explicit density-based solver of the compressible Navier–Stokes and energy conservation equations. Friction-induced heating was found to increase significantly when decreasing the pressure. At the same time, the Joule–Thomson cooling effect was calculated for up to 25 degrees K for the local fuel temperature drop relative to the fuel's feed temperature. The extreme injection pressures induced fuel jet velocities in the order of 1100 m/s, affecting the formation of coherent vortical flow structures into the nozzle's sac volume [13].

Koukouvinis et al. have been investigated erosion development due to cavitation inside Diesel injectors. Two similar injector designs are discussed both in terms of numerical simulation and experimental results from X-ray CT scans. During the simulation, pressure peaks have been found in areas of vapor collapse, with magnitude beyond 4000 bar, which is higher than the yield stress of common materials employed in the manufacturing of such injectors. The locations of such pressure peaks correspond well with the actual erosion locations as found from X-ray scans. The present work was the first to correlate pressure peaks due to vapor collapse with erosion development in industrial injectors with moving needle including comparison with experiments [14].

Firuzi et al. have been investigated the effects of increasing spray cone angle and turbulence intensity on the performance and emission of heavy-duty diesel engine. The numerical results indicate that creating swirly flow inside the

nozzle decreasing penetration length while, fuel spray cone angle increasing during the injection process. The nozzle with spiral rifling like guides has better performance and lower emission compared to other nozzle geometries. In this case, the fuel consumption is decreasing 32 percent than cylindrical nozzle hole, while the engine power and its torque increasing 63 percent. In addition, the amount of nitrogen oxide (NO) and carbon monoxide (CO) for the spiral convergent conical nozzle geometry reducing 15 percent and 30 percent respectively than cylindrical nozzle hole while engine has no soot emission problem [15].

Aleiferis & Papadopoulos numerically investigated Diesel injector nozzle with moving needle were performed using transient RANS modeling with compressibility of all phases accounted for. A range of fuel injection and air chamber pressures and temperatures were simulated, namely 400 and 900 bar upstream and 1, 35 and 60 bar downstream. Fuel, air and wall temperatures were varied in the range 300 K to 550 K. The results showed that the flow during injection carried hysteresis effects. After the end of injection, the state of the nozzle varied from being filled with a large amount of liquid to being filled mostly with air. Some form of immediate fuel dribble existed in all test cases, whilst late liquid fuel mass expulsion was also predicted under certain conditions. The latter prediction highlighted sensitivity to the models enabled. The use of a transient pressure outlet based on an engine's expansion stroke pressure trace affected the process of late fuel expulsion by pulling fuel out of the nozzle in multiphase form faster. These processes are of particular importance as they can contribute directly to unburned hydrocarbon emissions and/or the formation of deposits inside the holes. Starting a second injection from the resulting state of the nozzle at the end of the original injection resulted in a deformed liquid jet tip without the classic mushroom shape and a temporarily lower liquid jet penetration [16].

Ghobadian et al. have been optimized the EGR ratio, biodiesel fuel and operating conditions of a four-stroke single-cylinder diesel engine using the RSM method. In this study, using the EGR system, nitrogen oxide pollutants were reduced to a maximum of 63.7% for B10 fuel and 30% EGR ratio. Simultaneous use of biodiesel fuel and EGR system also reduces CO emissions at

different engine speeds [17].

Farajollahi et al. have been investigated the effect of the creation of swirly flow and the needle lift profile change on the behavior of the diesel fuel spray. The numerical results show that the conical nozzle hole has a longer penetration length than the cylindrical nozzle hole, but Sauter means the diameter of these two nozzles is almost the same. Also, these new nozzles have more spray cone angle and less penetration length and Sauter mean diameter than simple nozzles [18].

A review of previous articles shows that many studies have been done on the effect of different parameters on the performance and pollution of the combustion chamber, but so far the effect of simultaneous use of different nozzle geometries (converged & diverged conical) with different needle lift profiles and heat transfer study for injector multiphase flow, spray structure with indicated quantities on the performance and emission of soot, nitrogen oxide & carbon monoxide in the combustion chamber has not been done, which is in fact the main goal and innovation of the present article.

2) Injector - Spray simulation
The Eulerian-Eulerian model has been applied for simulating the multiphase flow inside the injector. The Eulerian-Lagrangian model has been employed to model the resultant spray. In this work, CRI1 diesel injector produced by Bosch companies, having five holes placed at equal spaces from each other, is used for modeling and simulation. The geometry of injector, created using CATIA software. In order to increase the accuracy and reduce the computation time, due to the symmetrical geometry of the injector, only 1/5 of cylindrical and convergent conical nozzle hole are simulated using AVL-Fire CFD code.

2.1) Governing equations
The governing equations are mass, momentum conservation, Energy, turbulence kinetic energy & dissipation rate [19].
Mass:

$$\frac{\partial \alpha_k \rho_k}{\partial t} + \nabla . \alpha_k \rho_k v_k = \sum_{l=1, k \neq l}^{N} \Gamma_{kl} , \text{k=1,...,N} \qquad (1)$$

In the above equation, α_k is the volume fraction of the phase k, v_k represents the velocity of phase k, and Γ_{kl} denotes the interfacial mass

exchange between the two phases of k and l. Furthermore, the convergence condition should satisfied [19]:

$$\sum_{k=1}^{N} \alpha_k = 1 \tag{2}$$

Momentum:

$$\frac{\partial \alpha_k \rho_k v_k}{\partial t} + \nabla . \alpha_k \rho_k v_k = -\alpha_k \nabla p + \nabla . \alpha_k (\vec{\tau}_k + \vec{T}^t_k) +$$

$$\alpha_k \rho_k \vec{f} + \sum_{l=1,k \neq l}^{N} M_{kl} + v_k \sum_{l=1,k \neq l}^{N} \Gamma_{kl}, \text{k=1,...,N} \tag{3}$$

In the above equation, f is the vector of volumetric force consisting of gravity and inertia forces, τ is the shear stress vector, T^t represents the Reynolds stress vector, M is the momentum exchange between two phases, and p denotes the static pressure [19].

Turbulence kinetic energy:

$$\frac{\partial \alpha_k \rho_k K_k}{\partial t} + \nabla . \alpha_k \rho_k v_k K_k = \nabla . \alpha_k (\mu_k + \frac{\mu_k^t}{\sigma_k}) \nabla K_k +$$

$$\alpha_k p_k - \alpha_k \rho_k \varepsilon_k + \sum_{l=1,k \neq l}^{N} K_{kl} + K_k \sum_{l=1,k \neq l}^{N} \Gamma_{kl}, \text{k=1,...,N} \tag{4}$$

Turbulence Dissipation Rate:

$$\frac{\partial \alpha_k \rho_k \varepsilon_k}{\partial t} + \nabla . \alpha_k \rho_k v_k \varepsilon_k =$$

$$\nabla . \alpha_k (\mu_k + \frac{\mu_k^t}{\sigma_k}) \nabla \varepsilon_k + \sum_{l=1,l \neq k}^{n} D_{kl} + \varepsilon_k \sum_{l=1,k \neq l}^{N} \Gamma_{kl} + \alpha_k c_1 p_k \frac{\varepsilon_k}{k_k}$$

$$-\alpha_k c_2 \rho_k \frac{\varepsilon_k^2}{k_k} +$$

$$\alpha_k c_4 \rho_k \varepsilon_k \nabla v_k, k = 1,...,N \tag{5}$$

Total Enthalpy Conservation:

$$\frac{\partial \alpha_k \rho_k h_k}{\partial t} + \nabla . \alpha_k \rho_k v_k h_k =$$

$$\nabla . \alpha_k (q_k + q_k^t) + \alpha_k \rho_k q_k^{''} + \alpha_k \rho_k f v_k +$$

$$\nabla . \alpha_k (\tau_k + \tau_k^t) v_k + \alpha_k \frac{\partial p}{\partial t} + \sum_{l=1,l \neq k}^{n} H_{kl} + h_k \sum_{l=1,l \neq k}^{n} \Gamma_{kl}, k = 1,...,N \tag{6}$$

q_k''' is the enthalpy volumetric source, H_{kl} represents the energy interfacial exchange between phases k and l.

2.2) Quantities Exchange

Three other equations (mass, momentum & enthalpy interfacial exchange) must be considered.

2.2.1) Mass exchange

The mass exchange between two phases is modeled using the nonlinear cavitation model [19]. The governing equation is as follows:

$$\Gamma_c = \rho_d N^{''} 4\pi R^2 \dot{R} = -\Gamma_d \tag{7}$$

N''' & R are numerical bubble density and bubble radius respectively. The bubble radius varying with time is obtained using the Rayleigh Equation as follows:

$$\dot{R} = \sqrt{\frac{2}{3}(\frac{\Delta p}{\rho_c} - R\ddot{R})} \tag{8}$$

In equation (6), Δp denotes the effective pressure difference and ρ_c represents the continuous phase density. Given the assumed linear descending ramp, the numerical bubble density is determined as follows:

$$N^{'''} = \begin{cases} N_0^{''} & \alpha_d \leq 0.5 \\ 2(N_0^{''} - 1)(1 - \alpha_d) + 1 & \alpha_d > 0.5 \end{cases} \tag{9}$$

Initial numerical bubble density(N_0'''), depends on the liquid phase properties and equals to 10^{12} for conventional diesel fuel [19].

2.2.2) Momentum exchange

The implemented interfacial momentum source includes the drag and turbulent dispersion forces:

$$M_c = \frac{1}{8} C_D \rho_c A_i^{''} |v_r| v_r + C_{TD} \rho_c k_c \nabla \alpha_d = -M_d \tag{10}$$

Here, C_D is the drag coefficient, v_r, denotes the relative velocity between two phases, C_{TD} represents the turbulent dispersion coefficient. Moreover, A''' denotes the density of interfacial area for the droplet and is calculated as follows [19]:

$$A_i^{''} = \pi D_b^2 N^{'''} = (36\pi N^{'''})^{\frac{1}{3}} \alpha_d^{\frac{2}{3}} \tag{11}$$

The drag coefficient force is a function of the bubble Reynolds number [19]:

$$C_D = \begin{cases} \frac{192}{Re_b}(1 + 0.1 Re_b^{0.75}) & Re_b \leq 1000 \\ 0.438 & Re_b > 1000 \end{cases} \tag{12}$$

2.2.3) Enthalpy exchange

The Ranz-Marshall heat exchange coefficient is based, as the name says, on the Ranz-Marshall correlation for the Nusselt number, Nu:

$$Nu = 2 + 0.6 Re_b^{\frac{1}{2}} Pr^{\frac{1}{3}} \tag{13}$$

Where Re_b is the local bubble Reynolds Number, and Pr is the Prandtl number. This model should be also used when the Ranz-Marshall correlation is employed in the calculation of mass exchange (boiling). The heat transfer rate becomes:

$$H_c = \frac{k_c}{D_d} Nu \cdot A_i^{''} (T_d - T_c) = -H_d \qquad (14)$$

Where k_c is the conductivity of the continuous phase (assumed to be liquid), and D_d is the dispersed phase (bubble/droplet) diameter. $A_i^{''}$ is the interfacial area density defined as:

$$A_i^{''} = \frac{6\alpha_d}{D_d} \qquad (15)$$

By given bubble/droplet diameter, D_d.

As said, the Eulerian–Lagrangian model has been applied for simulating the resultant spray. Momentum conservation equation has been used on a single droplet in a non-conservation form is:

$$m_d \frac{du_{id}}{dt} = F_{idr} + F_{ig} + F_{ip} + F_{ib} \qquad (16)$$

Where, F_{idr} is the drag force and equals to the following [20]:

$$F_{idr} = \frac{1}{2} \rho_g A_d C_d |u_{rel}| u_{irel} \qquad (17)$$

$$C_D = \begin{cases} \dfrac{24}{Re_d\, C_p}(1 + 0.15\,Re_d^{0.687})\,Re_d < 1000 \\[2mm] \dfrac{0.44}{C_p} \qquad\qquad\qquad Re_d \geq 1000 \end{cases} \qquad (18)$$

The acceleration of the droplet in a gaseous medium is as follows:

$$\frac{du_{id}}{dt} = \frac{3}{4} C_D \frac{\rho_g}{\rho_d} \frac{1}{D_d} |u_g - u_d|(u_{ig} - u_{id}) + (1 - \frac{\rho_g}{\rho_d}) g_i \qquad (19)$$

3) CFD Model

Injector different parts naming are shown in Figure 2. To consider the effect of nozzle hole geometry on the heat transfer, indicated quantities of diesel engine, the cylindrical nozzle hole is replaced with convergent and divergent conical nozzle as shown in Figure 3. Injector needle are shown in Figure 4. The geometry of the injector, created by AVL-Fire software, and the meshing of this geometry is performed using AVL-Fire software and shown in Figure 5. The impact of mesh size on the outlet mass flow rate and mean velocity of the fuel spray is studied to consider the grid study of the solution. The outlet mass flow rate & mean velocity from the injector nozzle becomes relatively stable at 76000 cells for cylindrical and conical nozzle holes. In this work, conventional diesel used as the liquid fuel and its properties are given in this refrence [21].
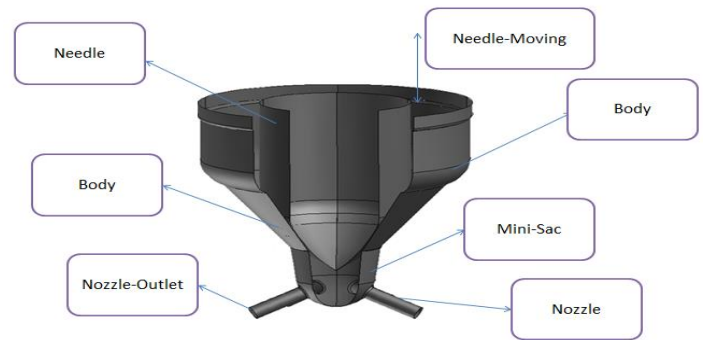

Figure 2: Injector Different Parts Naming

Cylindrical	Diverged Conical	Converged Conical
D_{in}=0.13	D_{in}=0.117	D_{in}=0.143 mm
D_{out}=0.13	D_{out}=0.13 mm	D_{out}=0.13mm
L=0.7 mm	L=0.7 mm	L=0.7 mm
r=2 μm	r=2 μm	r=10 μm

Figure 3: Injector Different Nozzle Geometries and Dimensions [12]
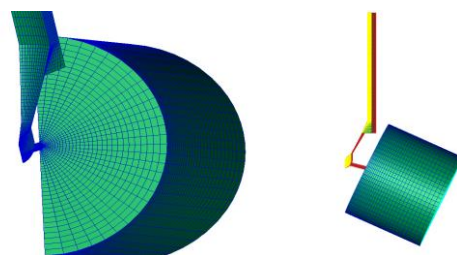

Figure 4: Injector needle

Figure 5: injector & spray mesh, (e) spray box mesh, nozzle and mini sac interface

Needle movement is corresponding with the 18 degree (0.8 ms) of the crank angle as shown in Figure 6 for different needle movement where lift-1 (triangular) is the base needle lift. Profiles 2 and 3 to investigate the effect of changing the slope of the needle displacement diagram at the

time of opening and closing and also the effect of injector needle opening time on the liquid fuel flow behavior inside the injector, mass flow rate from the nozzle, cavitation and hydrodynamic behavior of the fuel nozzle Diesels have been selected. The k-zeta-f turbulence model is utilized in simulation. The initial and boundary conditions for simulation of the injector are shown in Table 1 & Figure 7. In order of coupling the pressure and velocity fields, the SIMPLE algorithm has been employed. Spray simulation sub-model, Spray Break up simulation sub-models and nozzle sub-models are presented in table 2_4.

Table 1: Initial and boundary conditions of the flow inside the injector [12]

I.C.		B.C.		
Pressure	1350 bar	Inlet	Injection pressure	1350 bar
Temperature	313 K	Outlet	Outlet pressure	10 bar
		Inlet	Injection temperature	313 K
		Wall	Nozzle	Adiabatic

Table 2: Spray simulation sub-models [20]

Turbulent dispersion model	Enable
Particle interaction model	O-Rourke
Wall interaction model	Disable
Evaporation model	Dukowicz
E1	1
E2	1

Table 3: Spray Break up simulation sub-models [20]

Break up model	Wave
Model Constant C1	0.61
C2	20
C3	1
C4	0
C5	0
C6	0
C7	0
C8	0

Figure 6: Injector needle movement versus crank angle for different profiles [12]
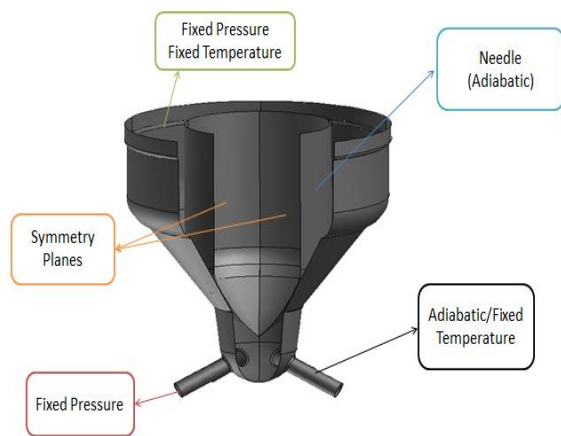
Figure 7: Injector Different Boundary Conditions [15]

Table 4: Nozzle sub-models [19]

Radial perturbation	Disable
Nozzle flow simulation	Disable
Boost hydraulics interface	Disable
Primary break up	Blob injection
Model Constant C1	0.61
C2	12
C3	2
C4	10
C5	1
C6	0.3
C7	0.03
C8	10
C8	0.188
C8	1
C8	1

4) Validation – Spray Results

The spray penetration length and Sauter mean diameter numerical data related to the cylindrical and convergent conical nozzle holes are compared to the existing experimental data [23] in order to consider the accuracy of the

numerical results obtained from simulating the injector and resulting spray. A good agreement is found between the results of present study and experimental data, as shown in Figure 8.
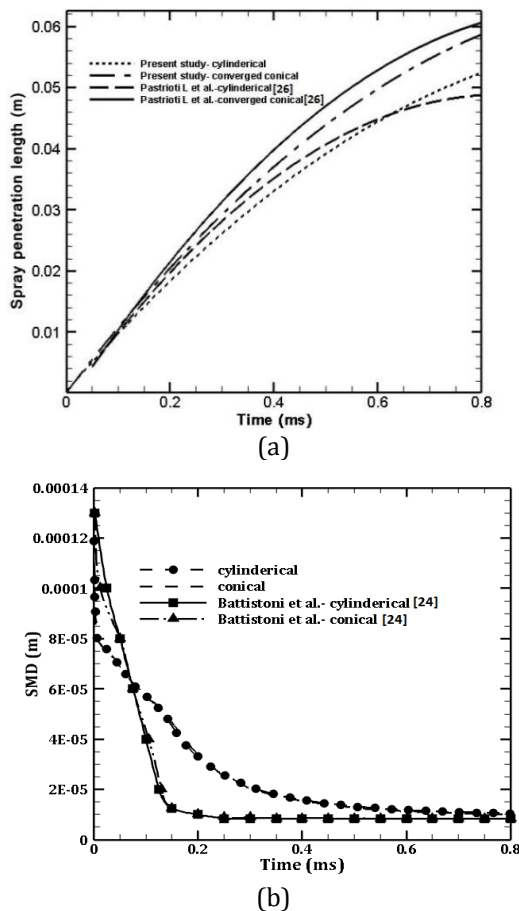

(a)

(b)

Figure 8: Validation of spray numerical results [23], (a) spray tip penetration length, (b) sauter mean diameter

5) Discussion on Results (Injector - Spray)
The plot of liquid volume fraction for different nozzle holes geometries and different needle movement profiles is displayed in Figure 9. According to this diagram, cavitation phenomenon has occurred in different geometries and profiles with different intensities and changing the needle displacement profile in different nozzle hole geometries has played an important role on the intensity of this phenomenon. The convergent conical nozzle hole has a larger diameter and radius of the input curve than the holes of the divergent cylindrical and conical nozzles, and therefore cavitation occurs with less intensity in the same displacement profile. Increasing the diameter and radius of the inlet hole of the nozzle leads to a decrease in pressure drop inside the nozzle hole and therefore cavitation

occurs with less intensity in this case. Due to the uniform radius of the inlet curve of cylindrical and divergent conical nozzles, reducing the inlet diameter of the divergent conical nozzle leads to an increase in the occurrence of cavitation and a decrease in the volume fraction of the liquid phase compared to other geometries. Another parameter that affects the intensity of cavitation is the needle displacement profile.

According to Figure 9, the volume fraction of the liquid phase at the end time of spraying the lift profile 3 with different nozzle holes geometries is more than the lift 2 profile with different nozzle holes geometries. By increasing the slope of the needle displacement diagram at the moment of its closure, the amount of fluid flow pressure inside the nozzle increases relatively slightly and the pressure drop decreases. Therefore, in this case, cavitation occurs with less intensity and the volume fraction of the liquid phase increases. Also, reducing the slope of the displacement diagram of the lift 3 profile in the initial moments of its closure has led to an increase in the pressure drop inside the nozzle hole and as a result, the volume fraction of the liquid phase has decreased.
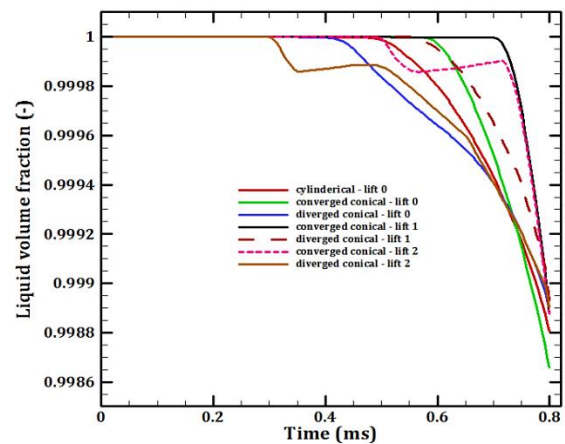

Figure 9: Liquid Volume Fraction during injection process for various nozzle holes geometries and different needle lifts

In order to investigate the simultaneous effect of changing the geometry and needle displacement profile on the hydrodynamic behavior of the fuel nozzle, compare the penetration length and average particle diameter, which are the most important characteristics of the fuel nozzle, and on the performance of the marine diesel engine. Production capacity, pollutants and specific fuel

consumption are influential, paid for in each section. Figure 10 shows the diagram of the average nozzle output velocity and diagram of the mass flow rate of the output in each case. Divergent cylindrical and conical cylinders have higher average output speeds. The reason for this is that the diameter and radius of the inlet curve of the converging conical nozzle hole are larger than the other two holes. By increasing the diameter and radius of the inlet curve of the nozzle hole, the amount of friction losses inside it decreases and therefore the average output velocity increases. Also, increasing the velocity at the nozzle output leads to increasing the output mass flow. The convergent conical nozzle has a higher output mass flow than the other modes. In the case of changing the needle displacement profile, due to the fact that the lift 2 and lift 3 profiles have a greater slope in the opening and closing moments than the base 1 profile, so the friction losses within it.

(a)

(b)
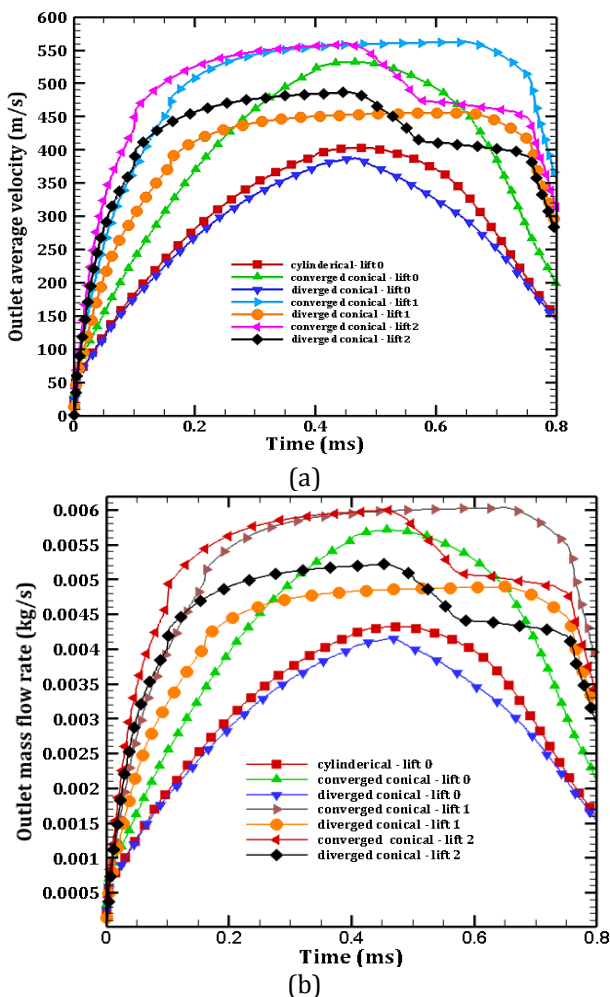
Figure 10: (a) Average velocity at nozzle outlet & (b) Outlet mass flow rate for various nozzle holes geometries and different needle lifts

Decreased and the average velocity of the nozzle output increases, which has led to an increase in the mass flow rate of the nozzle output. Also, in the new displacement profiles, the openness of the injector needle has increased compared to the base state, which has resulted in an increase in the mass flow rate of the nozzle output. The results for the discharge coefficient during the fuel injection time for each case are shown in Figure 11. In the injector nozzle, the discharge coefficient is a dimensionless parameter which is expressed as the ratio of numerical mass flow rate to maximum theoretical mass flow rate:

$$C_d = \frac{\dot{m}}{\dot{m}_{th}} = \frac{\dot{m}}{A_{th}\sqrt{2\rho_f \Delta p}} \qquad (20)$$

The velocity coefficient is expressed as the ratio of the numerical mean velocity to the maximum velocity of Bernoulli theory:

$$C_v = \frac{v_{avg}}{\sqrt{2\dfrac{\Delta p}{\rho_f}}} \qquad (21)$$

In the above equations, A_o is the cross section of the nozzle outlet, ρ_l is the density of the liquid fuel and Δp is the pressure difference between the inlet and outlet of the injector.

According to this figure, with increasing the intensity of cavitation and its development to the nozzle output, the discharge coefficient decreases and with decreasing the intensity of this phenomenon and less development or development of steam bubbles formed to the nozzle output, the discharge coefficient increases. Find. In fact, the occurrence and development of cavitation up to the nozzle output leads to a decrease in the cross-sectional area of the nozzle output and the intensity of cavitation has a significant effect on the value of this coefficient.

Figure 12 shows the results related to the penetration length and droplet diameter of the diesel fuel fountain in each case. Due to this shape, in the case of the same needle displacement profile, the convergent conical nozzle hole has a longer penetration length than other geometries, which is due to the increase in the average nozzle output speed due to the larger diameter and radius of the injector nozzle inlet curve. And reduce friction losses. By changing the needle displacement profile and increasing the slope of the diagram at the moment of opening and closing and increasing the opening time of the injector needle, due to

the reduction of friction losses inside the nozzle hole, the average output velocity increased and as a result the penetration length of the resulting fountain increased.
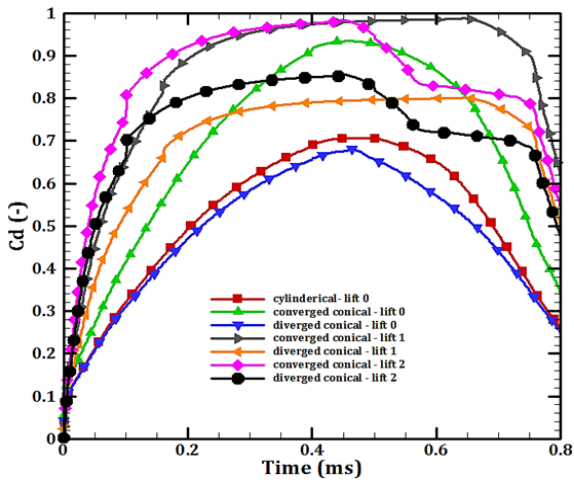

(a)
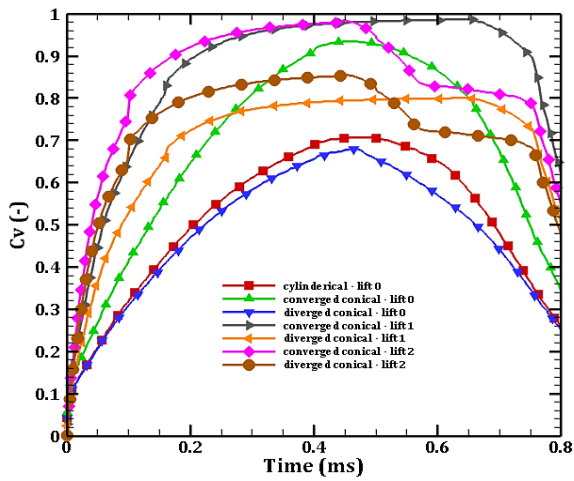
(b)

Figure 11: (a) Discharge coefficient and (b) velocity coefficient for various nozzle holes geometries and different needle lifts

The results for the amount of mass sprayed and evaporated into the combustion chamber are shown in Figure 13. The average particle diameter sizes for the three convergent, divergent, and cylindrical conical nozzle holes are approximately equal. Cavitation occurs in the holes of divergent cylindrical and conical nozzles and in the convergent cone holes the increase in the average velocity of the nozzle leads to the improvement of the fuel jet collapse and finally the average particle diameter size is reduced. As the average velocity at the nozzle outlet increases, the relative velocity between the nozzle particles and the dense air inside the combustion chamber increases, resulting in an

increase in the drag aerodynamic force leading to the collapse of the fuel nozzle and a decrease in the average particle diameter. In the case of changing the needle displacement profile, due to the increase in the average velocity at the nozzle outlet, the aerodynamic force increases and as a result, the collapse of the fountain occurs with more intensity and leads to a further decrease in the average particle diameter size compared to the same profile. As the nozzle output mass flow rate increases due to the change in the needle displacement profile, the amount of mass sprayed into the combustion chamber increases. Also, with the increase of the sprayed mass inside the combustion chamber, the amount of evaporated mass also increased and as a result, the average diameter of the particles also decreased more in this case. The results related to the calculated fountain structure inside the constant volume cylindrical combustion chamber in each case at the end time of the spray are given in Figure 19.
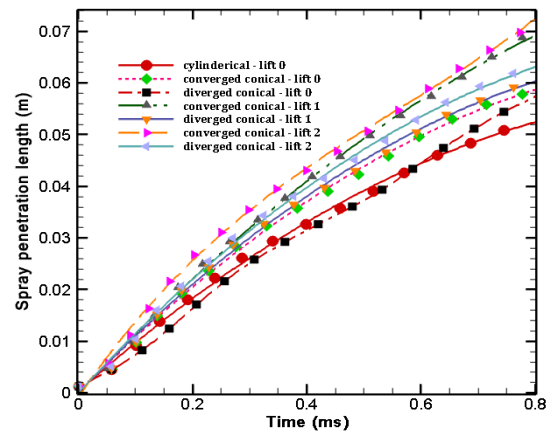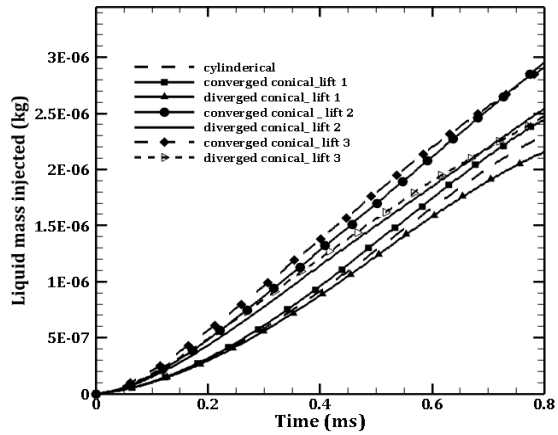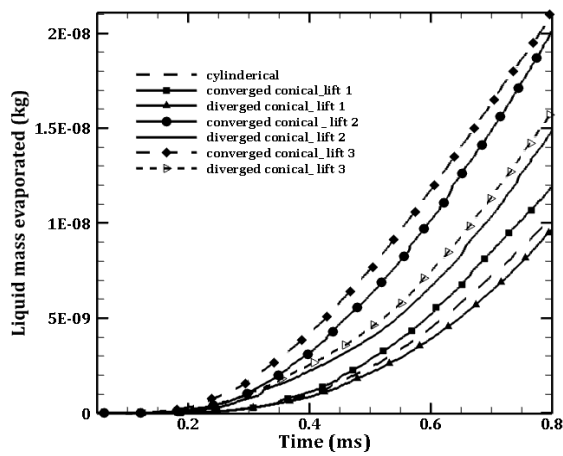

(a)
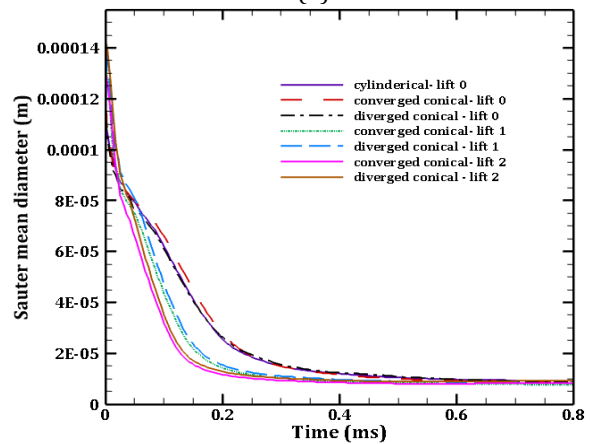
(b)

Figure 12: (a) Spray penetration length & (b) Sauter mean diameter (SMD) for various nozzle holes geometries and different needle lifts

(a)

(b)

Figure 13: (a) liquid mass injected & (b) liquid mass evaporated for various nozzle holes geometries and different needle lifts

Flow streamline inside the injector nozzle for various nozzle holes geometries and different needle lifts presented in Figure 14. Vapor fuel volume fraction distribution inside nozzle and spray structure for various nozzle holes geometries and different needle lifts presented in Figures 15-16.

Mean temperature & Mean pressure inside the injector during the injection process are presented in Figures 17-19.
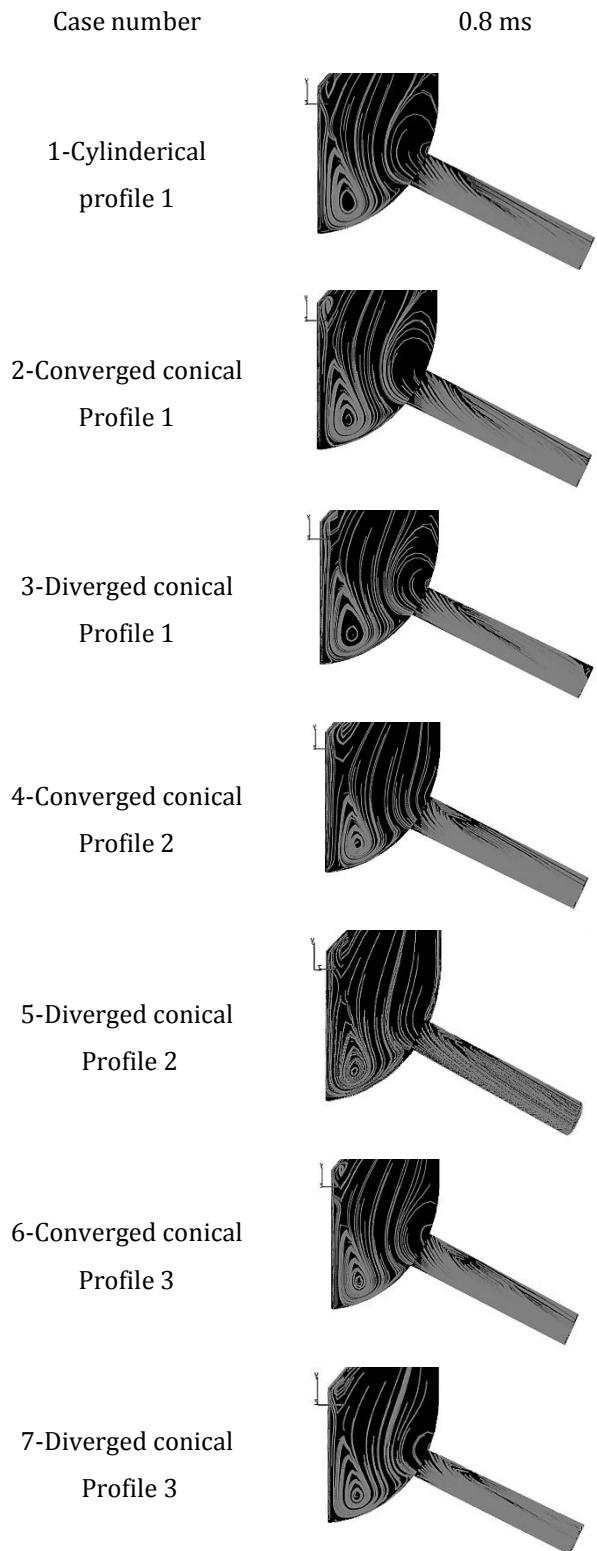
Case number	0.8 ms
1-Cylinderical profile 1	
2-Converged conical Profile 1	
3-Diverged conical Profile 1	
4-Converged conical Profile 2	
5-Diverged conical Profile 2	
6-Converged conical Profile 3	
7-Diverged conical Profile 3	

Figure 14: Flow streamline inside the injector nozzle for various nozzle holes geometries and different needle lifts

0.8 ms

Cylinderical lift 0

Converged conical lift 0

Diverged conical lift 0

Converged conical lift 1

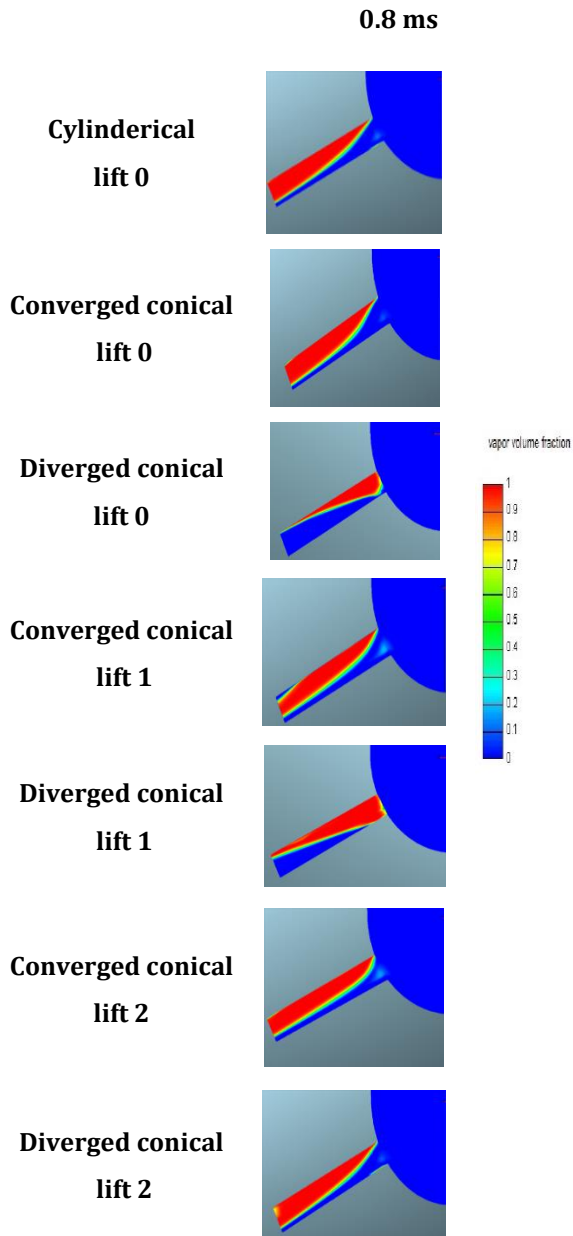**Diverged conical lift 1**

Converged conical lift 2

Diverged conical lift 2

Figure 15: Vapor fuel volume fraction distribution inside nozzle for various nozzle holes geometries and different needle lifts
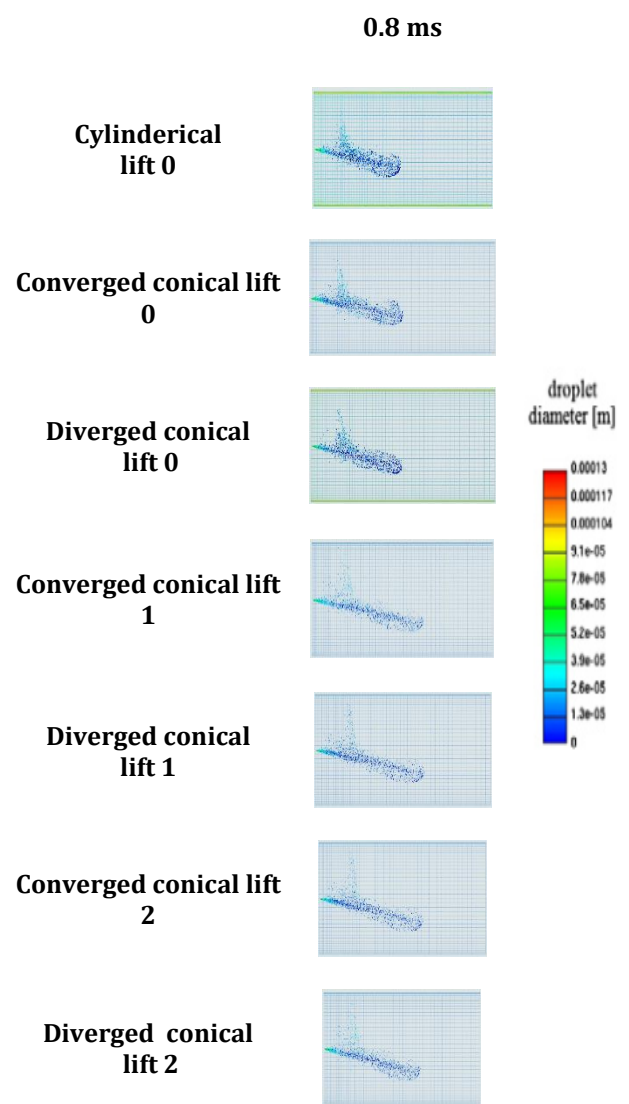
0.8 ms

Cylinderical lift 0

Converged conical lift 0

Diverged conical lift 0

Converged conical lift 1

Diverged conical lift 1

Converged conical lift 2

Diverged conical lift 2

Figure 16: Spray structure inside the combustion chamber for various nozzle holes geometries and different needle lifts

(a)   (b)
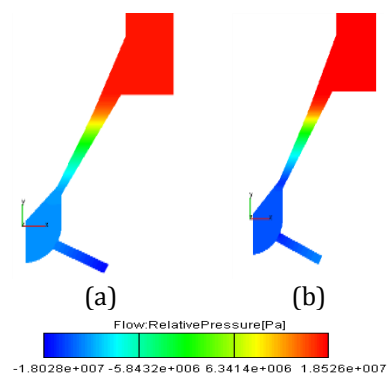
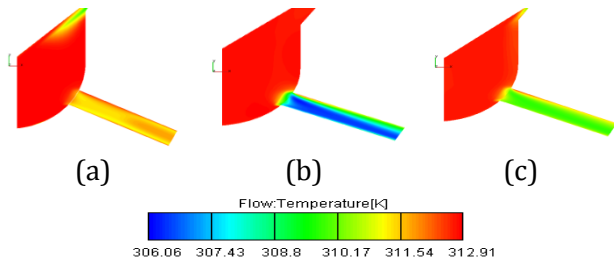Figure 17: Relative Pressure Contours simple nozzle (start & end of injection)

Figure 18: Temperature distribution inside nozzle for various nozzle holes geometries and different needle movement profiles (a)-(c) cylindrical nozzle @ start-center & end time of injection

6) Engine Simulations

The Eulerian- Lagrangian model is applied to simulate the engine cycle. A diesel engine with its conventional injector is simulated in order to study the effect of nozzle hole geometry change and swirly flow creation inside the injector nozzle on the efficiency, performance and pollution of diesel engine. AVL-Fire software is utilized for the three-dimensional modeling.

6.1) Governing equations

The governing equations are conservation of mass, momentum, and energy. In these types of diesel engines, several terms are added to the mass, momentum, and energy conservation relationships due to the injection of fuel spray inside the cylinder [24].

Mass conservation equation:

$$\frac{\partial \rho}{\partial t} + \sum_i \frac{\partial}{\partial x_i}(\rho v_i) = S_m \tag{22}$$

Where, S_m represents the generation of mass due to the evaporation of fuel spray droplets [24].

Momentum conservation equation (Navier-Stokes Equation):

$$\frac{\partial (\rho v_i)}{\partial t} + \sum_{j=1}^{3} \frac{v_j \partial (\rho v_i)}{\partial x_j} =$$
$$\sum_{j=1}^{3} \frac{\partial \tau_{ij}}{\partial x_j} - \frac{\partial P}{\partial x_i} + \rho F_{v,i} + F_{p,i} \tag{23}$$

$F_{v,i}$ presenting volume forces, $F_{p,i}$ mostly represents the pressure force in the multiphase flow, and τ_{ij} represents the shear stress [24]:

Energy conservation equation:

$$\frac{\partial (\rho h)}{\partial t} + \sum_{j=1}^{3} \frac{\partial (\rho v_j h)}{\partial x_j} = \sum_{j=1}^{3} \frac{\tau_{ij} \partial v_i}{\partial x_j} + \frac{\partial P}{\partial t}$$
$$+ v_i \frac{\partial P}{\partial x_i} - \sum_i \frac{\partial q_i}{\partial x_i} + S_h \tag{24}$$

In the above relationship, h is the enthalpy, e is the internal energy per unit mass, and q is the heat flux along i due to temperature gradient. S_h is the energy generated due to the evaporation of spray droplets.

6.2) Engine CFD Model
6.2.1) Combustion - Emission

Diesel engine geometry creation and meshing are performed using the ESE Diesel module. The specifications of the diesel engine and its spray and the properties of the air inside the cylinder at the start of compression process are extracted from refrence [12]. Boundary conditions in engine simulation presented in table 5.

Table 5: Boundary conditions in engine simulation [12]

Boundary Condition	Value
Cylinder head surface temperature	550.15 K
Wall surface temperature	475.15 K
Piston surface temperature	575.15 K

Models used in engine combustion & pollution simulation are presented here:

Table 6: Model used in engine combustion & pollution simulation [12]

Pressure-Velocity coupling	Simple-Piso
Combustion	ECFM-3Z
Turbulence	k-zeta-f
Primary Break up	viscous droplet
Secondary Break up	standard wave
Evaporation	Dukowicz
Wall interaction	Wall Jet-1
laminar flame speed	Metghalchi and Keck
NO formation	Extended Zeldovich
Soot formation & Oxidation	Kennedy/Hiroyasu/Magnussen

Due to engine symmetric geometry, only 1/6 of the geometry is simulated in order to reduce the computation time and price. The simulation begins at the closure of the air intake valve (IVC) and ends at the opening of the exhaust valve (EVO). It is worth mentioning that this mesh has 67564 cells in TDC as shown in Figure 19.
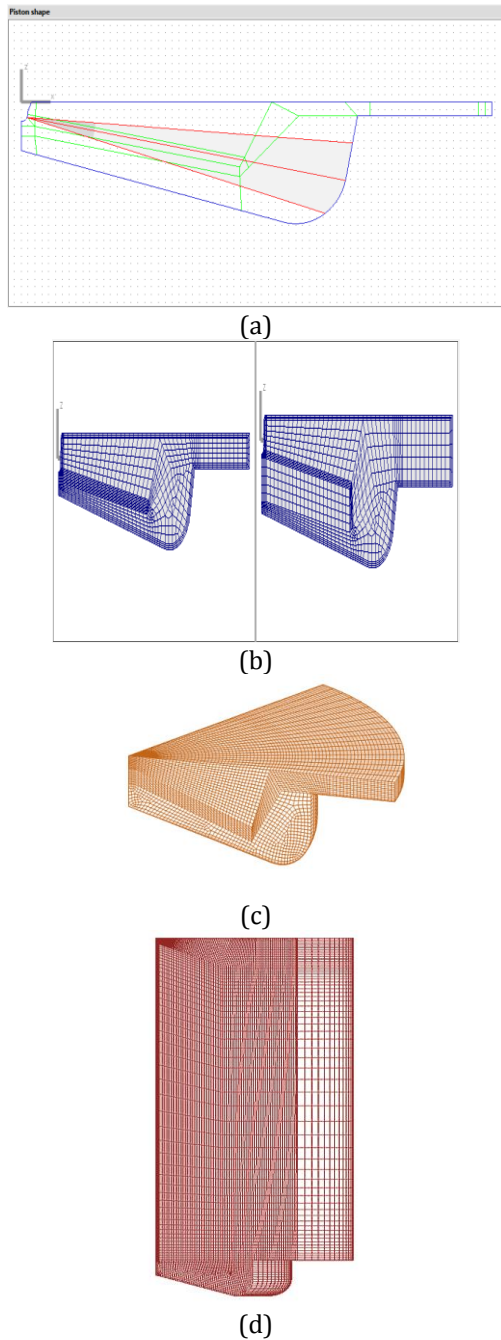
(a)

(b)

(c)

(d)

Figure 19: Engine grid, (a) 2D blocking structure, (b) 2D moving mesh, (c) 3D mesh @ TDC and (d) 3D mesh @ BDC

6.3) Validation - Engine Results

The numerical results are compared to experimental data in order to determine their accuracy. Figure 20 shows a plot of the mean pressure inside the combustion chamber and the rate of heat released versus crank angle for the simulated model and reference [25]. As seen in this figure, a very good agreement exists between them.

6.4) Engine with different needle lift and geometries

Engine is simulated with various other injector nozzle holes geometries, using the file stored from the injector simulation. It is worth noting that the engine parameters such as rotational speed, fuel injection start time (SOI), injection pressure, compression ratio and geometry are constant; however, the injection duration (DOI), the injected fuel mass, fuel injection end (EOI) time and spray characteristics are variable due
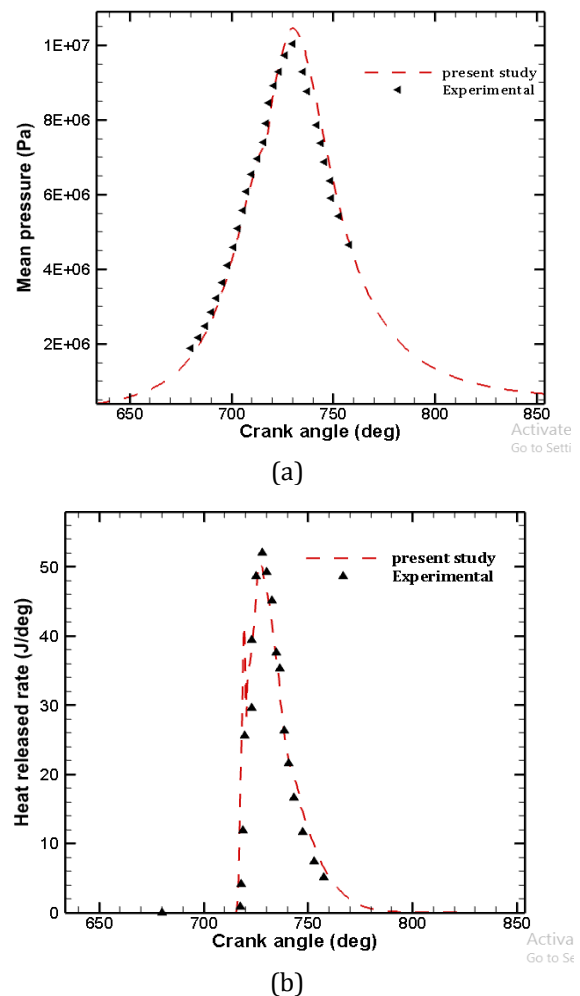

(a)

(b)

Figure 20: Validation of the numerical results of engine simulation using empirical and numerical results, (a) mean pressure & (b) rate of heat released inside the combustion chamber [25]

to various nozzle hole geometries & different needle movement profiles.

## 6.5) Discussion (combustion – emission)

Convergent conical nozzle hole has the highest injected fuel mass. Figure 21 displays the effects of different nozzle holes geometries on the

mean pressure and temperature inside the ICE cylinder, respectively. Since all the conditions at the beginning of compression and the engine geometry are identical for all cases, the injected fuel mass and the combustion efficiency are the factors causing difference in maximum mean pressure and temperature at different cases. A rise in the combustion efficiency improves the knock rating, resulting in higher mean temperature and pressure inside the combustion chamber. Moreover, a larger fuel mass injected into the engine chamber is equivalent to more energy, also leading to larger equivalence ratio, temperature and pressure inside the combustion chamber. This corresponds to a better combustion behavior in this geometry compared to others due to better spray characteristics. The indicated power, torque, and specific fuel consumption (SFC) for one working cycle of the engine are shown for various nozzle holes geometries and different needle movement profiles in Table 7. It can be concluded from comparing the numerical results that the engine performance improves by changing the nozzle holes geometry from cylindrical to convergent and changing needle lift. Numerical results show that converged conical with trapezius needle lift profile has better engine performance, efficiencies and low NO pollution. Although, diverged conical with trapezius needle lift profile has lower CO pollution. Fuel consumption decreases by 18.5% and its power and torque increase 64%. Also in this case, carbon monoxide pollutants decrease by 14% and nitrogen oxide pollutants decreasing by 10% for optimum status. In this case, indicated and mechanical efficiencies are increasing 22% and 41.5% respectively. General engine emission results for various cases at engine EVO are shown in table 8. Diverged conical with triangular needle lift profile has worst engine performance, efficiencies and higher NO pollution. Although, converged conical with triangular needle lift profile has higher CO pollution. Fuel consumption increases by 2.75% and its power and torque decreasing 10.5 and 8.5%. Also in this case, carbon monoxide pollutants increases by10% and nitrogen oxide pollutants increases by 6%. In this case, indicated and mechanical efficiencies are decreasing 3.7% and 10.41% respectively. Figure 22 shows the nitrogen oxide & CO emission versus crank angle for various states. Figure 23 displays the amount of

soot emission & non- reactive equivalence ratio versus crank angle in various states. As shown in this figure, the soot is well oxidized and eliminated at the end of the combustion process for all injector nozzle hole geometries.
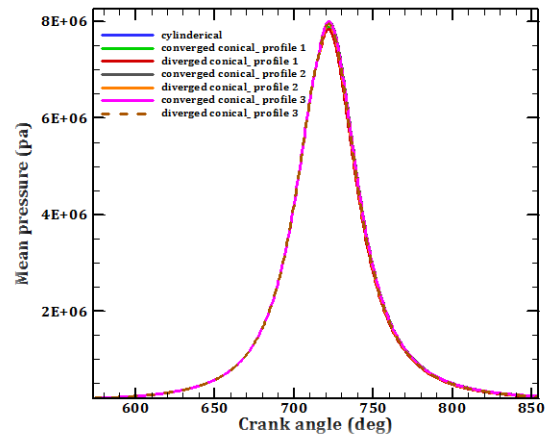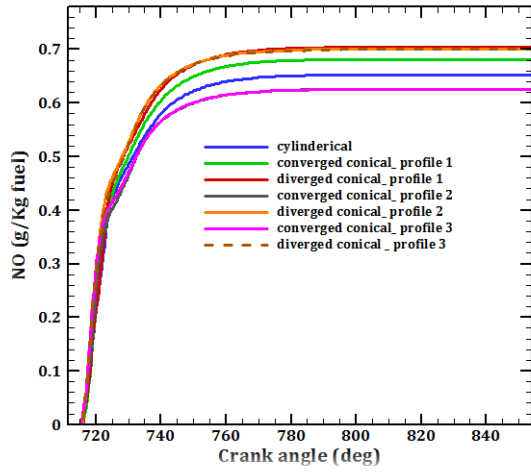

(a)
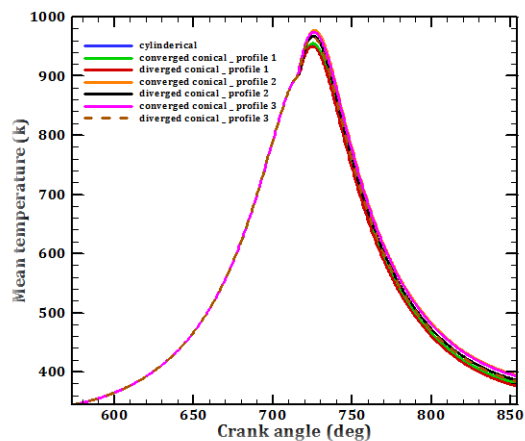
(b)

Figure 21: In cylinder mean pressure (a) & Mean temperature (b) different geometry and needle movement profiles

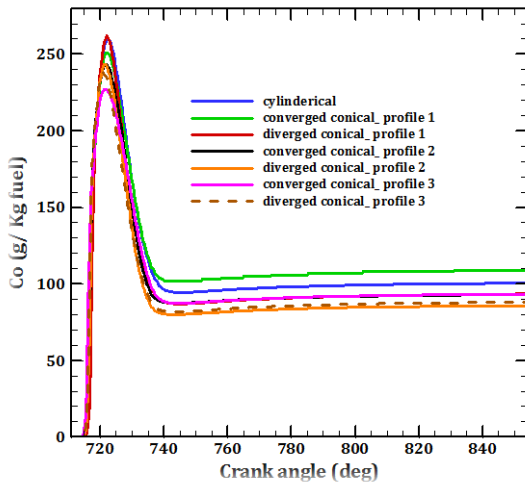Table 7: General engine indicated quantities for various cases

Case Number	Indicated power (KW)	Indicated torque (Nm)	SFC(Kg/KW-h)
1	1.92	11.47	0.3166
2	2.1	12.56	0.3073
3	1.75	10.47	0.3254
4	3.16	18.85	0.2575
5	2.52	15.03	0.2757
6	3.01	17.96	0.2626
7	2.36	14.11	0.2835

Table 8: General engine emission results for various cases at engine output

Case Number	NO (g/kg-fuel)	CO (g/kg-fuel)
1	0.66	100
2	0.68	110
3	0.70	93.5
4	0.62	93.2
5	0.70	85.9
6	0.62	93.5
7	0.70	88.1

and gradually moves toward the cylinder wall. temperature locations and soot forms mostly in low-temperature locations. These two pollutants show opposite behavior, and with a decrease in one, the other increases.
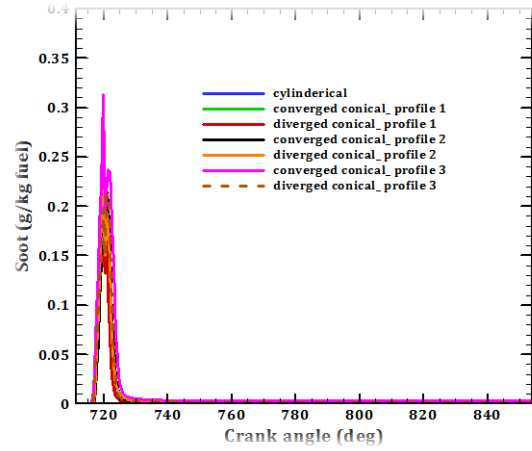
(a)

(b)

Figure 23: Soot mass fraction (a) & equivalence ratio (b) for different geometry and different needle movement profiles

(a)

(b)

Figure 22: NO mass fraction (a) & CO mass fraction (b) for different geometry and different needle movement profiles
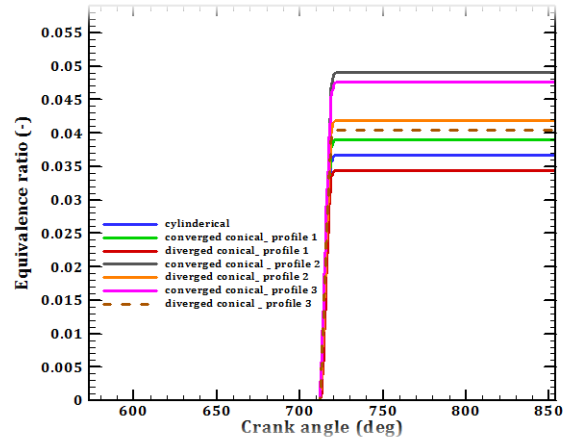
Also, indicated & mechanical efficiency & Air-fuel, Excess air ratio & Injected fuel mass for different geometry & needle movement profiles are presented in table 9-10.

Figure 24 shows the two-dimensional contours of temperature distribution inside the cylinder. As shown, combustion begins from the center

Table 9: Indicated & Mechanical efficiency for different geometry & needle movement profiles

Case Number	Indicated efficiency (%)	Mechanical efficiency (%)
1	27	48
2	28	52
3	26	43
4	33	68
5	31	60
6	32	67
7	30	58

Table 10: Air-fuel, Excess air ratio & Injected fuel mass for different geometry & needle movement profiles

Case Number	Air-fuel ratio (-)	Excess air ratio (-)	Injected fuel mass (m-gr)
1	392.87	27.25	127
2	369.7	25.64	13.5
3	418.81	29.05	11.9
4	294.05	20.4	16.9
5	344.34	23.88	14.5
6	302.55	20.98	16.5
7	356.8	24.75	14

Figs. 25 and 26 display two-dimensional contours of nitrogen oxide and soot mass fraction, respectively. As seen in these figures, nitrogen oxide forms mostly in high-
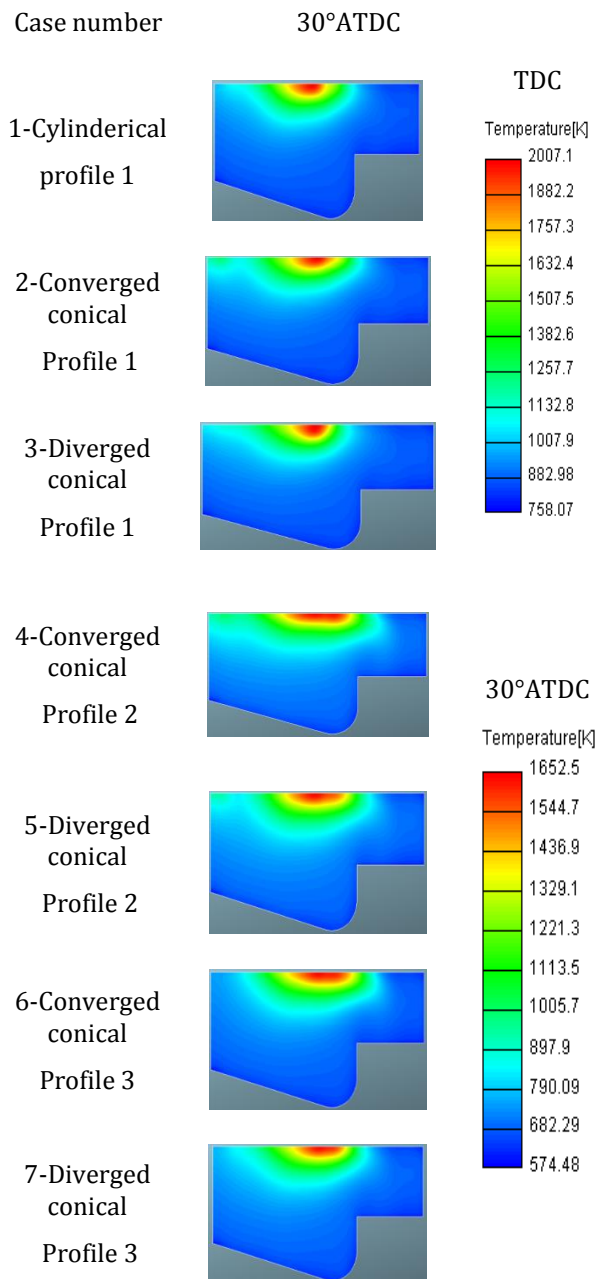
Figure 24: Temperature distribution inside the cylinder at two different angles (30° ATDC)
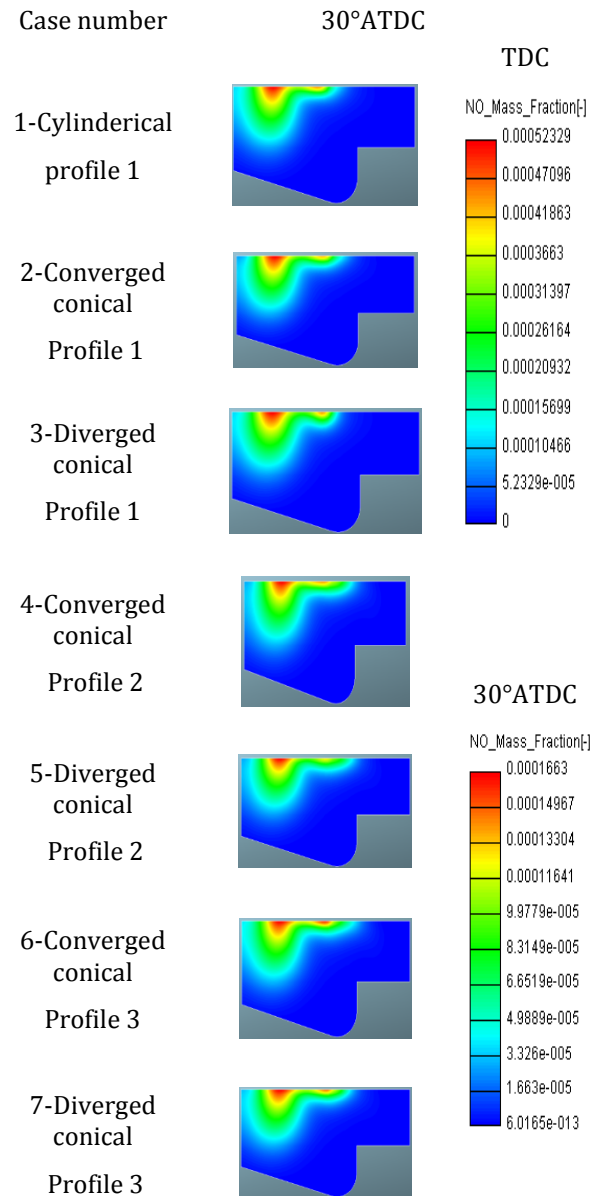

Figure 25: Distribution of nitrogen oxide mass fraction inside the cylinder at two different angles (30° ATDC)

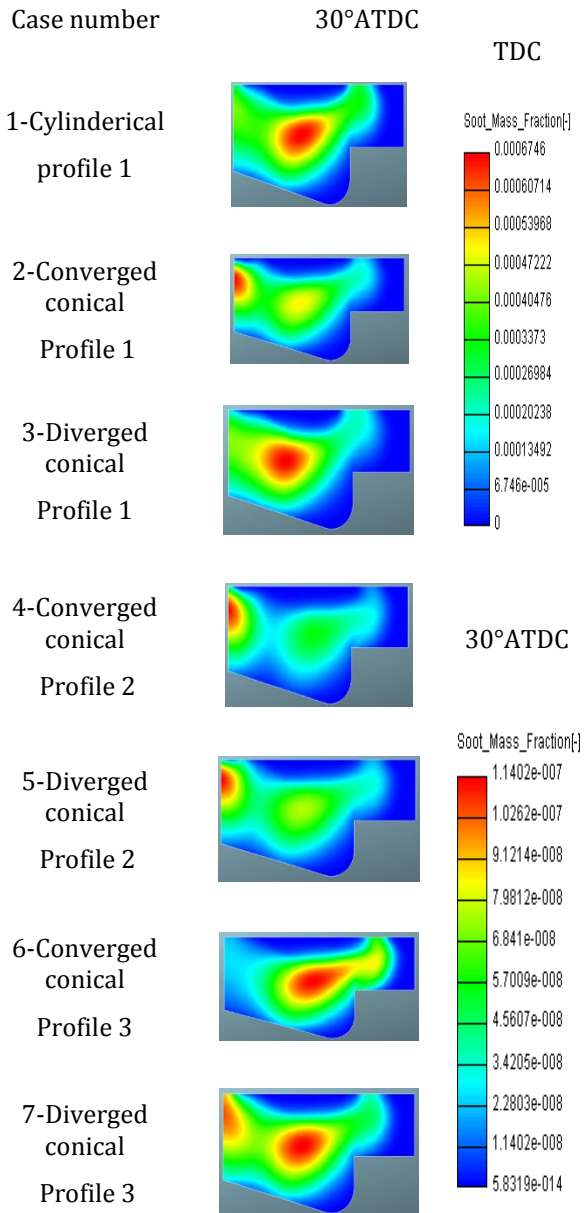Figure 26: Distribution of soot mass fraction inside the cylinder at two different angles (30° ATDC)

Figure 27: Distribution of CO mass fraction inside the cylinder at two different angles (30° ATDC)

Although carbon monoxide is generated during combustion process for rich mixtures, but a small part of carbon monoxide is also released under lean conditions. Figure 27 shows the two-dimensional contours of CO distribution inside the cylinder for two different crank angles.
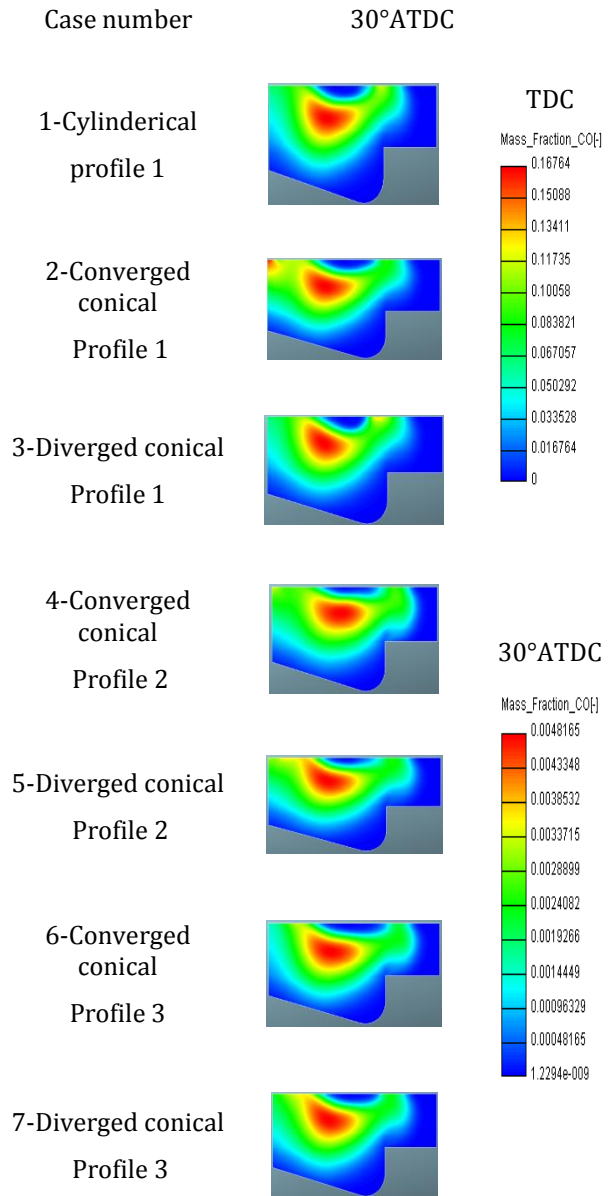
7) Conclusion

In the present paper, the effect of using Different Orifice Geometries & Needle Lifts profiles on transient heat-mass transfer and Combustion Indicated Quantities & Air Pollutant Species has been investigated in Marine Propulsion System Fuel Injectors using AVL-Fire CFD code. The effect of each of the proposed geometry and needle movement profiles by numerical model in AVL Fire software, which has been validated with experimental data in each part, on the performance & Air Pollutant Species of the Marine Propulsion System has been investigated. Numerical results show that

converged conical with trapezius needle lift profile has better engine performance, efficiencies and low NO pollution. Although, diverged conical with trapezius needle lift profile has lower CO pollution. It can be concluded from comparing the numerical results that the engine performance improves by changing the nozzle holes geometry from cylindrical to convergent and changing needle lift. Numerical results show that converged conical with trapezius needle lift profile has better engine performance, efficiencies and low NO pollution. Although, diverged conical with trapezius needle lift profile has lower CO pollution. Fuel consumption decreases by 18.5% and its power and torque increase 64%. Also in this case, carbon monoxide pollutants decrease by 14% and nitrogen oxide pollutants decreasing by 10% for optimum status. In this case, indicated and mechanical efficiencies are increasing 22% and 41.5% respectively. Although, converged conical with triangular needle lift profile has higher CO pollution. In this case, carbon monoxide pollutants increases by10% and nitrogen oxide pollutants increases by 6%. In marine diesel engines, the penetration length of the sprayed fuel must be proportional to the geometry of the combustion chamber in order to form a better fuel-air mixture and also to prevent it from colliding with the engine wall. Because if it hits the piston and the cylinder walls, the amount of unburned hydrocarbons will increase and the engine efficiency will decrease. Also, if the penetration length is shorter, a weak fuel-air mixture is formed. Therefore, cavitation intensity and nozzle outlet velocity play an important role in improving fuel atomization phenomenon and controlling fuel jet characteristics by simultaneously changing the nozzle holes geometry and needle displacement profile due to their role on marine diesel performance and pollution is important.

Acknowledgement

References

[1] J.B. Heywood, Internal Combustion Engine Fundamentals, McGraw-Hill, Inc., New York, 1998.

[2] F.J. Salvador, J. Martínez-López, M. Caballer and C. De Alfonso, Study of the Influence of the Needle Lift on the Internal Flow and Cavitation Phenomenon in Diesel Injector Nozzles by CFD Using RANS Methods, Energ. Conversion. Manage, Vol. 66, No. 2, pp. 246-256, 2013.

[3] C. Yao, C. Cheung, C. Cheng and Y. Wang, Reduction of Smoke and Nox from Diesel Engines Using A Diesel/Methanol Compound Combustion System, Energ . Fuels, Vol. 21, No. 2, pp. 686-691, 2007.

[4] C. Yao, P. Geng, Z. Yin, J. Hu, D. Chen and Y. Ju, Impacts of Nozzle Geometry on Spray Combustion of High Pressure Common Rail Injectors in A Constant Volume Combustion Chamber, Fuel, Vol. 179, No. 1, pp. 235-245, 2016.

[5] S. Som, S.K. Aggarwal, E.M. El-Hannouny and D.E. Longman, Investigation of Nozzle Flow and Cavitation Characteristics in A Diesel Injector, J. Eng. Gas. Turb. Power, Vol. 132, pp. 1–12, 2010.

[6] S. Som, D.E. Longman, A.I. Ramirez and S.K. Aggarwal, Influence of Nozzle Orifice Geometry and Fuel Properties on Flow and Cavitation Characteristics of A Diesel Injector, In: Lejda Kazimierz, editor, Fuel injection in automotive engineering, InTech, ISBN: 978-953-51-0528-2, 2012.

[7] C. Soteriou, R. Andrews and M. Smith, Direct Injection Diesel Sprays and the Effect of Cavitation and Hydraulic Flip on Atomization, SAE Technical Paper 950080, 1995.

[8] H.K. Suh and C.S. Lee, Effect of Cavitation in Nozzle Orifice on the Diesel Fuel Atomization Characteristics, Int. J. Heat. Fluid. FL, Vol. 29, pp.1001–1009, 2008.

[9] F. Payri, V. Bermúdez, R. Payri and F.J. Salvador, The Influence of Cavitation on the Internal Flow and the Spray Characteristics in Diesel Injection Nozzles, Fuel, Vol. 83, pp. 419–431, 2004.

[10] R. Payri, F.J. Salvador, J. Gimeno and J. dela Morena, Study of Cavitation Phenomena Based on A Technique for Visualizing Bubbles in A Liquid Pressurized Chamber, Int. J. Heat. Fluid. FL, Vol. 30, pp. 768–777, 2009.

[11] S. George, K. Phoevos, T. Andreas, G. Manolis and B. George, Transient Heating Effects in High Pressure Diesel Injector Nozzles, International Journal of Heat and Fluid Flow, 2014.

[12] A.H. Farajollahi, R. Firuzi, M. Rostami and A. Mardani, Numerical Study on the Effects of Creating Rotationary Flow Inside the Injector

Nozzle and Changing Fuel Injection Angle on the Performance and Emission of Caterpillar Diesel Engine, Journal of the Brazilian Society of Mechanical Science and Engineering, Vol. 44, No. 3, pp. 1-17, 2022.

[13] K. Konstantinos, K. Phoevos, M. Robert and G. Manolis, Transient Cavitation and Friction-Induced Heating Effects of Diesel Fuel during the Needle Valve Early Opening Stages for Discharge Pressures up to 450 MPa, Energies, 2021.

[14] K. Phoevos, G. Manolis, L. Jason and W. Lifeng, Large Eddy Simulation of Diesel injector including cavitation effects and correlation to erosion damage, Fuel, Vol. 175, pp. 26–39, 2016.

[15] A.H. Farajollahi, R. Firuzi, M. Rostami and F. Bagherpoor, Consideration of the Effects of Increasing Spray Cone Angle and Turbulence Intensity on Heavy-Duty Diesel Engine Pollution and Specific Outputs Using CFD, International Journal of Engine Research, Article in Press, 2022.

[16] P.G. Aleiferis and N. Papadopoulos, Heat and Mass Transfer Effects in the Nozzle of A Fuel Injector from the Start of Needle Lift to After the End of Injection in the Presence of Fuel Dribble and Air Entrainment, International Journal of Heat and Mass Transfer, Vol. 165, pp. 120576, 2021.

[17] F. Jaliliantabar, B. Ghobadian and Najafi, G., Optimizing the EGR Rate, Biodiesel Fuel Ratio and Engine Working Mode Using RSM Method, Journal of fuel and combustion, Vol. 10, No.03, pp. 15-31, 2016.

[18] A.H. Farajollahi, R. Firuzi, M. Pourseifi, A. Mardani and M. Rostami, Numerical Investigation of the Effect of Swirl and Needle Lift Profile Change on the Diesel Fuel Spray Behavior, Journal of Engine Research, Vol. 54, pp. 25-38, 2019.

[19] Avl List GmbH. AVL Fire v. 2013, CFD solver, Eulerian multiphase, 2013.

[20] Avl List GmbH. AVL Fire v. 2013, CFD solver, Spray, 2013.

[21] N.I. Kolev, Multiphase Flow Dynamics 3: Turbulence, Gas Absorption and Diesel Fuel Properties, Springer, 2007.

[22] A.H. Farajollahi and R. Firuzi, Numerical Investigation on the Effect of Creating Swirly Flow Inside the Nozzle and Injection Pressure Increase on the Cavitation and Diesel Fuel Spray Characteristics, Mechanical Engineering, Vol. 51, No. 3 , pp. 155-164, 2020.

شبیه سازی جریان چندفازی انژکتور موتور و کمیت اندیکاتوری برای هندسه های مختلف نازل و حرکت سوزن

رضا فیروزی ۱*، فرید باقرپور ۲، امیرحمزه فرج الهی ۳

۱ کارشناس ارشد تبدیل انرژی، دانشگاه بین المللی امام خمینی، ایران، *rezafiruzi@edu.ikiu.ac.ir*

۲ دکترا دانشگاه امام علی (ع)، تهران، ایران، *farid.bagherpor@gmail.com*

۳ استادیار دانشگاه امام علی (ع)، تهران، ایران، *a.farajollahi@sharif.edu*

* نویسندۀ مسئول

چکیده

در مقاله حاضر، تأثیر استفاده از هندسه‌های مختلف دهانه و بالابرهای سوزنی بر انتقال گذرا جرم گرما و مقادیر نشان‌دهنده احتراق و گونه‌های آلاینده هوا در انژکتورهای سوخت سیستم محرکه دریایی با استفاده از کد AVL-Fire CFD مورد بررسی قرار گرفته است. تأثیر هر یک از پروفیل‌های هندسی پیشنهادی و حرکت سوزن (مثلثی، ذوزنقه‌ای و چکمه‌ای) با کمک یک مش متحرک سه‌بعدی بهوسیله مدل عددی در نرم‌افزار AVL Fire که با داده‌های آزمایشی در هر قسمت تأیید شده است، بر روی عملکرد و گونه های آلاینده هوا سیستم پیشران دریایی توسط ماژول ANALYZER بررسی شده است. نتایج عددی نشان می دهد که مخروطی همگرا با پروفیل بالابر سوزنی ذوزنقه ای عملکرد موتور، راندمان و آلودگی کمتر NO را دارد. اگرچه، مخروطی واگرا با پروفیل بالابر سوزنی ذوزنقه دارای آلودگی CO کمتری است. مصرف سوخت ۱۸٫۵ درصد کاهش می یابد و قدرت و گشتاور آن ۶۴ درصد افزایش می یابد. همچنین در این حالت آلاینده‌های مونوکسید کربن ۱۴ درصد و آلاینده‌های اکسید نیتروژن ۱۰ درصد کاهش می‌یابند تا وضعیت بهینه به دست آید. در این حالت راندمان نشان داده شده و بازده مکانیکی به ترتیب ۲۲٪ و ۴۱٫۵٪ افزایش می‌یابد.